Journal of Nuclear Materials 384 (2009) 81–86

Contents lists available at ScienceDirect

Journal of Nuclear Materials

journal homepage: www.elsevier.com/locate/jnucmat

# Thermal studies on fluorite type $Zr_yU_{1-y}O_2$ solid solutions

N.K. Kulkarni [a], K. Krishnan [a], U.M. Kasar [b], S.K. Rakshit [b], S.K. Sali [a,*], S.K. Aggarwal [a]

[a] Fuel Chemistry Division, Bhabha Atomic Research Centre, Trombay, Mumbai 400 085, India
[b] Product Development Division, Bhabha Atomic Research Centre, Trombay, Mumbai 400 085, India

ARTICLE INFO

*Article history:*
Received 18 July 2008
Accepted 19 October 2008

ABSTRACT

Solid state reactions of $UO_2$ and $ZrO_2$ in mild oxidizing condition followed by reduction at 1673 K showed enhanced solubility up to 35 mol% of zirconium in $UO_2$ forming cubic fluorite type $Zr_yU_{1-y}O_2$ solid solution. The lattice parameters and O/M (M = U + Zr) ratios of the solid solutions, $Zr_yU_{1-y}O_{2+x}$, prepared in different gas streams were investigated. The lattice parameters of these solid solutions were expressed as a linear equation of $x$ and $y$: $a_0$ (nm) = 0.54704 − 0.021$x$ – 0.030$y$. The oxidation of these solid solutions for $0.1 \leqslant y \leqslant 0.2$ resulted in cubic phase $MO_{2+x}$ up to700 K and single orthorhombic zirconium substituted $\alpha$-$U_3O_8$ phase at 1000 K. The kinetics of oxidation of $Zr_yU_{1-y}O_2$ in air for $y$ = 0–0.35 were also studied using thermogravimetry. The specific heat capacities of $Zr_yU_{1-y}O_2$ ($y$ = 0–0.35) were measured using heat flux differential scanning calorimetry in the temperature range of 334–860 K.



## 1. Introduction

$UO_2$ is known to form substitutional solid solution with oxides of tetravalent (Th, Np, Pu), trivalent (rare earths), divalent (Mg, Ca, Sr) and monovalent (Li and Na) metal atoms [1–5]. Among all these oxides, tetravalent elements are natural substituents since uranium occur as $U^{4+}$ in $UO_2$ and these elements are expected to form complete range (0–100 mol%) of solid solution with $UO_2$. However, $ZrO_2$ forms a limited range of solid solution with $UO_2$ because of mismatch in ionic sizes of $Zr^{4+}$ (0.084 nm) and $U^{4+}$ (0.10 nm) and difference in the structures of $UO_2$ and $ZrO_2$. Zirconia ($ZrO_2$) is having monoclinic structure at room temperature, transforms to tetragonal phase at 1443 K and to cubic (fluorite type) phase at 2643 K. In general, size of the metal ion, oxidation state, electronegativity and structure are the important factors which limit the solubility of metal oxide in $UO_2$. The solubility of $ZrO_2$ in actinide oxides increases with decrease in size of actinide ion. Thus the solid solubility of $ZrO_2$ in $ThO_2$, $UO_2$ and $PuO_2$ is 5, 15 and 80 mol%, respectively at 1673 K. However, the solubility of $ZrO_2$ in $UO_2$ matrix increases from 15 to 35 mol% with increase in temperature from 1673 K to 2148 K. $ZrO_2$ forms fluorite type cubic solid solution $(U,Zr)O_2$ for higher concentration of uranium ($UO_2$ > 85 mol%) and tetragonal type solid solution $(U,Zr)O_2$ for higher concentration of zirconium ($ZrO_2$ > 85 mol%) and these two phases are separated by two phase region [6]. The complete phase diagram of $UO_2$–$ZrO_2$ system was evaluated by calculation of phase diagram (CALPHAD) method [7].

Zirconia based ceramics (fluorite) are being considered as promising matrices for actinides disposal [8]. $UO_2$–$ZrO_2$ system has received considerable attention because of possible use of cubic $(U,Zr)O_2$ solid solution as a nuclear fuel. Also in a hypothetical case of nuclear severe accident, the reactor core could melt and form a mixture, called corium which mainly consists of $UO_2$ and $ZrO_2$. The physical, chemical and/or thermodynamic properties of such solid solutions are considerably different from those of $UO_2$ and are affected not only by metal content but also by the oxygen non-stoichiometry. The crystal chemistry, thermodynamic and magnetic properties of fluorite type solid solutions $M_yU_{1-y}O_{2+x}$ (M = $M^{2+}$, $M^{3+}$ and $M^{4+}$) in uranium dioxide host lattice have been reviewed by Fujino and Miyake [9]. The crystal chemical study of solid solution $M_yU_{1-y}O_{2+x}$ in relation with metal ion concentration and oxygen non-stoichiometry, is important to understand behavior of nuclear fuel during irradiation. The lattice parameters of $M_yU_{1-y}O_{2+x}$ are linearly related to metal ion concentration and O/(M+U) [9]. Une and Oguma [10] have reported a single phase region of the solid solution $Zr_yU_{1-y}O_2$ in $0 \leqslant y \leqslant 0.15$ at 1773 K and $0 \leqslant y \leqslant 0.35$ at 2148 K [11]. The lattice parameter change ($da$) of the solid solution with metal ion concentration ($y$), $da/dy$, does not agree in these reports. The reported values of $da/dy$ are –0.027 for specimen prepared at 1773 K [10], −0.0294 at 1998 K [12] and −0.0301 at 1923 K [13]. No data about the change of lattice parameter with oxygen non-stoichiometry, $da/dx$, have been given in these reports. The oxygen potential of $Zr_yU_{1-y}O_{2+x}$ solid solutions were measured for $y$ = 0.1, 0.15, 0.2 and 0.3 and $x$ values between 0.04 and 0.17 [10,14]. The addition of zirconium was reported to decrease oxygen potential of $UO_2$ and according to Hoch and Furman [15], the addition of $Zr^{4+}$ tends to oxidize $U^{4+}$ to $U^{5+}$, giving lower oxygen potential. High temperature heat capacities of $(U_{0.91}M_{0.09})O_2$ (M = Pr,

* Corresponding author. Fax: +91 22 25505151.
*E-mail address:* sksali2002@yahoo.com (S.K. Sali).

0022-3115/$ - see front matter © 2008 Published by Elsevier B.V.
doi:10.1016/j.jnucmat.2008.10.015

Ce and Zr) measured by direct heating pulse calorimetry have also been reported over the temperature range 290 to 1410 K [16].

This paper describes the work carried out on solid solubility of $ZrO_2$ in $UO_2$. Single phase region of the solid solution was studied by X-ray powder diffraction method. The lattice parameter change in this region was expressed as a linear function of $x$ and $y$ of $Zr_yU_{1-y}O_{2+x}$. The oxidation behavior of these solid solutions was studied using thermogravimetry. The specific heat capacities of $Zr_yU_{1-y}O_2$ for $y = 0.1$, 0.2, 0.3 and 0.35 were measured using heat flux type differential scanning calorimeter (DSC).

## 2. Experimental

### 2.1. Material synthesis

$ZrO_2$ (BDH 99.9%) and $UO_{2.00}$ were used as starting materials. Stoichiometric uranium oxide, $UO_{2.00}$, was obtained by reduction of nuclear grade $U_3O_8$ in a stream of purified argon gas with 8% (v/v) hydrogen gas mixture at 1073 K for 3 h. Weighted amounts of $UO_{2.00}$ and $ZrO_2$ were intimately mixed in an agate mortar with small amount of ethyl alcohol. Zr (mol%) in the mixtures were 10, 20, 30, 35 and 40. The samples with corresponding compositions were also prepared by gel combustion method using standard solutions of uranyl nitrate and zirconium nitrate with glycerol as a fuel. The solution was evaporated to dryness and then decomposed in air at 1073 K for 3 h to remove residual carbon. The heated product was reduced in Ar/8% $H_2$ at 1073 K for 5 h. The homogenous mixtures obtained in both the solid state and the solution route were pressed at 2 t/cm$^2$ into pellets of 7 mm diameter and 4 mm height, the weight being about 1 g. The pellets were placed in an alumina boat and heated in SiC resistance furnace in a stream of commercial argon at 1673 K for 48 h. The products obtained after this heat treatment were reground and pressed into pellet and further heated in Ar/8% $H_2$ (v/v) atmosphere at 1673 K for about 10 h. The end products obtained after each heat treatment were analyzed by X-ray powder diffraction (XRD) method. The diffractometer experiments were carried out on a STOE instrument using Cu K$\alpha$ radiation ($\lambda = 0.15406$ nm) monochromatized with graphite monochromator placed between specimen and NaI(Tl) scintillation detector. The estimated error in lattice parameter was ±0.0002 nm.

### 2.2. Characterization

The non-stoichiometry ($x$) in $Zr_yU_{1-y}O_{2+x}$ was obtained by chemical analysis for U(IV) and total uranium. For the analysis of total uranium, Fe (II) was used for reduction of U(VI) to U(IV) in concentrated phosphoric acid medium [17]. Un-reacted excess iron (II) was oxidized with dil. $HNO_3$ in presence of molybdenum (VI) as catalyst and U(IV) was titrated with potassium dichromate solution potentiometrically. U(IV) was determined by direct titration with $K_2Cr_2O_7$. The entire titration was carried out on weight basis.

Thermograms of $Zr_yU_{1-y}O_{2.00}$ for $y = 0.1$, 0.2, 0.3, 0.35 and 0.4 were recorded using Mettler Thermoanalyzer (model: TGA/SDTA851$^e$/MT5/LF1600) in flowing dry air at a heating rate of 10 K min$^{-1}$ up to 1473 K. The thermoanalyzer was calibrated from the weight loss obtained for the decomposition of ~100 mg of $CuSO_4 \cdot 5H_2O$ to CuO during heating to 1273 K. Calculated and the experimental weight loss values were in good agreement indicating reliability of the measurement. Non-isothermal oxidation kinetics of $Zr_yU_{1-y}O_{2.00}$ ($y = 0.0$, 0.2 and 0.35) were studied in air up to 1073 K at a heating rate of 4 K min$^{-1}$.

Molar heat capacity measurements were carried out using a heat flux type differential scanning calorimeter (DSC 131, SETARAM, France). Temperature calibration for the calorimeter was done by using the phase transition temperatures of NIST reference materials (indium: $T_{fus} = 429.748$ K; tin: $T_{fus} = 505.078$ K; lead: $T_{fus} = 600.600$ K; mercury: $T_{fus} = 234.316$ K). Analar grade samples of potassium nitrate ($T_{trs} = 400.850$ K) and silver sulfate ($T_{trs} = 703.150$ K) were also used to perform temperature calibration of DSC. Heat calibration of the calorimeter was carried out using the heats of transition of above-mentioned materials. Standard molar heat capacity of $Zr_yU_{1-y}O_{2.00}$ (s) for $y = 0.1$, 0.2, 0.3, 0.35 was measured, in duplicate, for each composition in the temperature range of 334–860 K. Heat flows as a function of temperature were measured in the temperature range from 334 to 860 K at a heating rate of 5 K min$^{-1}$ with high purity argon as a carrier gas and a flow rate of 2 dm$^3$ h$^{-1}$.

To determine the heat capacity as a function of temperature in continuous heating mode, three sets of experiments were performed. In all the experiments, parameters such as initial and final temperature, heating rate, delay time and the carrier gas (argon) flow rate were kept constant. In the first experiment, two empty cylindrical flat bottom aluminum crucibles of identical masses of capacity $10^{-4}$ dm$^3$ with covering lids were kept inside the furnace over the crucible holders. In the second experiment, heat flow as a function of temperature was measured by taking a known weight (~200 mg) of powdered NIST synthetic sapphire (SRM-720) sample into the aluminum crucible kept in the sample crucible side and keeping the empty crucible in the reference side. In a similar way, heat flow as a function of temperature was measured by taking a known weight (~200 mg) of $Zr_yU_{1-y}O_{2.00}$(s) powder sample. Heat capacity of sample under investigation was calculated using the expression:

$$C_p(T)_{sample} = \{(HF_{Sample} - HF_{Blank})/(HF_{Ref} - HF_{Blank})\} \cdot (M_{Ref}/M_{Sample}) \cdot C_p(T)_{Ref}, \quad (1)$$

where $HF_{Blank}$, $HF_{Ref}$ and $HF_{Sample}$ represent heat flows during first, second and third experiments, respectively. $C_p(T)_{Sample}$ and $C_p(T)_{Ref}$ denote the heat capacities of sample and reference materials. $M_{sample}$ and $M_{Ref}$ stand for the mass of sample and reference, respectively. In order to check the accuracy of the measurement, heat capacity of $Fe_2O_3$ (mass fraction 0.9999) was measured in the temperature range from 334 to 860 K. The heat capacity of NIST synthetic sapphire (SRM-720) sample used in the calculation was taken from the literature [18]. The value of heat capacity of $Fe_2O_3$(s) was found to be within ±2% in the temperature range (334–860 K) of the values reported in the literature [18].

## 3. Results and discussion

### 3.1. Synthesis and XRD studies of $Zr_yU_{1-y}O_2$

The powder XRD patterns of black products obtained on heating various ratios of $UO_2$:$ZrO_2$ in argon and then on reduction in Ar/8%$H_2$(v/v) at 1673 K were fluorite type (fcc), similar to that of $UO_2$. The unit cell parameters of the fluorite type phases obtained from solid state as well as gel combustion method were identical. Fig. 1 shows the lattice parameter of the fcc phase as a function of zirconium concentration obtained on heating in argon and then in Ar/8%$H_2$ atmosphere at 1673 K. It can be seen that lattice parameters of the fcc phase obtained on heating in argon are lower than those obtained after heating in Ar/8%$H_2$ atmosphere. Also the lattice parameter decreases linearly with increase in zirconium concentration up to 35 mol% of $ZrO_2$ in both the cases. The lattice parameter decreases linearly from 0.54704 nm for pure $UO_{2.00}$ to 0.5365 nm for $Zr_{0.35}U_{0.65}O_{2.00}$ indicating the solid solubility of $ZrO_2$ in $UO_2$ lattice. However, on further increase in zirconium concentration up to 40 mol%, tetragonal phase of $ZrO_2$ starts separating out along with the fcc phase, having unit cell parameter of

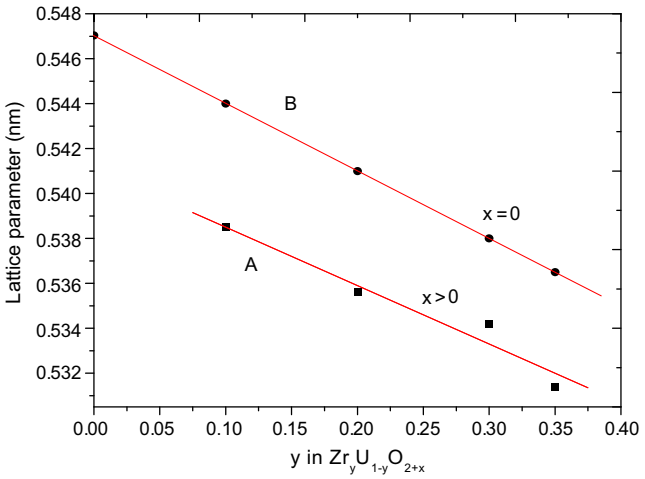


**Fig. 1.** Lattice parameter of cubic solid solutions, $Zr_yU_{1-y}O_{2+x}$, as a function of zirconium concentration obtained on heating in (A) Argon at 1673 K ($x > 0$) and (B) Argon at 1673 K followed by heating in Ar/8%$H_2$ at 1673 K ($x = 0$).

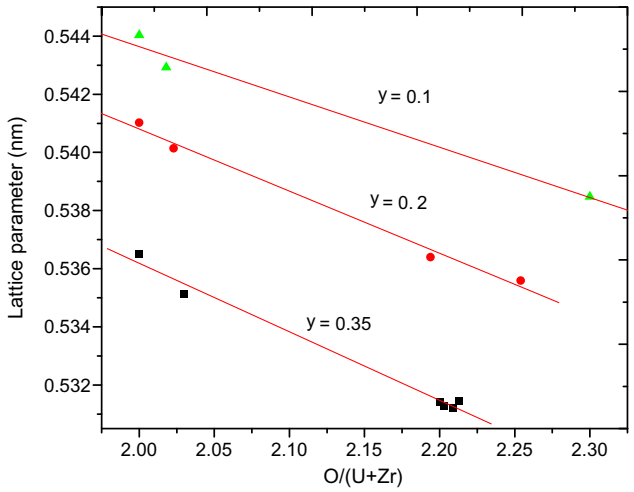


**Fig. 2.** Lattice parameter vs. O/(U+Zr) for $Zr_yU_{1-y}O_{2+x}$ for $y = 0.1$, 0.2 and 0.35.

0.5365 nm, indicating limiting composition of the single phase solid solution as $Zr_{0.35}U_{0.65}O_{2.00}$. The present observed unit cell parameters of $Zr_yU_{1-y}O_{2.00}$ ($y = 0.1$, 0.2, 0.3 and 0.35) obtained by the modified procedure agree well with the reported lattice parameter data for $(U,Zr)O_{2.00}$ solid solutions obtained by heating in hydrogen atmosphere up to 2148 K [11]. Normally, the solid solutions are prepared by direct heating of $UO_2$ and $ZrO_2$ mixtures in Ar/8%$H_2$ atmosphere for 4–10 h. However, in the present studies, the preparative conditions were modified. The oxide mixtures were initially heated in argon gas, containing 10–20 ppm of oxygen impurity, up to 1673 K for 48 h, before heating in Ar/8%$H_2$ up to 1673 K for 10 h.

A comparison of the unit cell parameters of the fcc phases obtained on heating in argon and after heating in Ar/8%$H_2$ atmosphere suggests two types of phases, namely, $Zr_yU_{1-y}O_{2+x}$ and $Zr_yU_{1-y}O_{2.00}$. The initial heating of $UO_2$ and $ZrO_2$ mixture in argon with 10–20 ppm of oxygen, leads to oxidation of $U^{4+}$ from $UO_{2.00}$ to $U^{5+}$ or $U^{6+}$ thereby decreasing the $UO_2$ lattice parameter. As the difference in ionic radii of $Zr^{4+}$ and $U^{5+}/U^{6+}$ is reduced, the solubility of $ZrO_2$ in $UO_2$ increases. This was further verified from the chemical analysis values of U(IV) and U(VI) in $Zr_yU_{1-y}O_{2+x}$ and $Zr_yU_{1-y}O_{2.00}$. In $Zr_yU_{1-y}O_{2+x}$, the U(IV)/U(VI) ratio depends on oxygen potential of the argon atmosphere and it increases drastically on reduction in Ar/8%$H_2$ atmosphere. Thus this modified method of heating the sample in two step heating process helps in increasing the solubility of $ZrO_2$ in $UO_2$ up to 35 mol% at 1673 K. In Fig. 1(A) and (B), the lattice parameters of $Zr_yU_{1-y}O_{2+x}$ and $Zr_yU_{1-y}O_{2.00}$ are linearly related to metal ion concentration ($y$) by a linear Eqs. (2) and (3) respectively,

$$a_0\ (\mathrm{nm}) = 0.5411 - 0.026y \text{ for } Zr_yU_{1-y}O_{2+x}, \quad (2)$$

$$a_0\ (\mathrm{nm}) = 0.54704 - 0.030y \text{ for } Zr_yU_{1-y}O_{2.00}. \quad (3)$$

Eq. (3) is in good agreement with those reported by Aroson and Clayton [12] and Hinatsu and Fujino [13]. However, slope of Fig. 1(A) shows that the rate of change of lattice parameter, $da/dy$, is different from 0.030 when the samples are heated in argon atmosphere. This is because of contribution of oxygen non-stoichiometry ($x$) to decrease in lattice parameter. The lattice parameters of cubic solid solutions are linearly related to metal ion and oxygen ion concentrations.

For correlation of lattice parameter ($a_0$) as a function of O/M (M = U + Zr) change ($x$), different $x$ values were obtained for a fixed metal ion concentration. These $x$ values were changed by using different oxygen concentrations in an inert gas stream and also by using different O/U ratios of the starting uranium oxide. Oxygen to metal ratios of the solid solutions were obtained from chemical analysis of U(IV) and total uranium. The U(IV)/$U_{total}$ ratio gives O/U, from which O/M is calculated assuming zirconium is present as $ZrO_2$. Fig. 2 shows plots of lattice parameter as a function of O/M ratio in $Zr_yU_{1-y}O_{2+x}$ for $y$ values of 0.1, 0.2 and 0.35. Three approximately parallel straight lines were obtained by linear regression with an average slope ($da/dx$) of −0.021. The coefficient of $x$ (for $x > 0$) reported for various solid solutions were −0.014 ($Th_yU_{1-y}O_{2+x}$) [1], −0.0131 ($La_yU_{1-y}O_{2+x}$) [19] and −0.0127 ($Pr_yU_{1-y}O_{2+x}$) [20]. These values of coefficient of $x$, (i.e. $da/dx$) are comparatively higher (less negative) as compared to a value of −0.021 determined in the present work. This may be due to smaller size of $Zr^{4+}$ as compared to that of $Th^{4+}$, $La^{3+}$ and $Pr^{3+}$ leading to the largest lattice contraction due to incorporation of $ZrO_2$ in $UO_2$.

Using the coefficient of $x$ as −0.021 and with the $UO_{2.00}$ lattice parameter being taken as 0.54704 nm [21], the correlation of lattice parameter with zirconium concentration ($y$) and oxygen non-stoichiometry ($x$) can be given as

$$a_0(\mathrm{nm}) = 0.54704 - 0.021x - 0.030y. \quad (4)$$

Table 1 shows a comparison of the experimental and calculated lattice parameters for $Zr_yU_{1-y}O_{2+x}$ using Eq. (4). The value of x was in the range 0.0–0.23. The agreement between the observed and calculated lattice parameter indicates validity of Eq. (4).

### 3.2. Oxidation behavior of $Zr_yU_{1-y}O_2$

Many studies on the air oxidation of un-irradiated $UO_2$ have been reported to define conditions (such as time and temperature) for safe handling and storage of used fuel [22]. The effect of dopants on the rate of oxidation of $UO_2$ has been studied to gain insight into difference in reactivity of $UO_2$ and used fuel. In order to investigate the progress of the oxidation reaction as a function of temperature, thermogravimetric studies on $Zr_yU_{1-y}O_2$ were carried out in air using heating rate of 10 K/min up to 1473 K. Figs. 3 and 4 show % weight gain **(or** O/U added as second axis**)** and DTG curves respectively, for oxidation of $Zr_yU_{1-y}O_2$ ($y = 0.1$–0.35). These figures show that oxidation behavior of $0.1 \leqslant y \leqslant 0.2$ and $0.3 \leqslant y \leqslant 0.35$ are not similar. Fig. 3(A) and (B) show two step oxidation in TG and DTG (Fig. 4(A) and (B)) for $y = 0.1$ and 0.2 respectively, up to 1000 K followed by slow mass loss in the temperature range 1000 to 1473 K. XRD pattern of 773 and 800 K heated product was fluorite type with values of lattice parameters as

**Table 1**
Comparison of experimental and calculated lattice parameters for $Zr_yU_{1-y}O_{2+x}$ a (nm) = 0.54704 − 0.021$x$ − 0.030$y$.

| zirconium concentration (Y) | U(IV)/$U_{total}$ (%) | O/U | O/ M = 2 + $x$ | $a_{obs}$ ± 0.0002 (nm) | $a_{cal}$ (nm) |
|---|---|---|---|---|---|
| 0.35 | 100 | 2.000 | 2.000 | 0.5365 | 0.5365 |
| 0.35 | 95.43 | 2.045 | 2.030 | 0.5352 | 0.5359 |
| 0.35 | 79.50 | 2.205 | 2.133 | 0.5333 | 0.5337 |
| 0.35 | 69.15 | 2.309 | 2.201 | 0.5314 | 0.5323 |
| 0.35 | 68.81 | 2.312 | 2.203 | 0.5313 | 0.5322 |
| 0.35 | 67.78 | 2.322 | 2.209 | 0.5312 | 0.5321 |
| 0.35 | 67.25 | 2.328 | 2.213 | 0.5315 | 0.5320 |
| 0.30 | 100 | 2.000 | 2.000 | 0.5380 | 0.5380 |
| 0.30 | 96.12 | 2.039 | 2.027 | 0.5379 | 0.5375 |
| 0.30 | 95.80 | 2.042 | 2.029 | 0.5374 | 0.5374 |
| 0.30 | 72.75 | 2.273 | 2.191 | 0.5335 | 0.5340 |
| 0.30 | 74.20 | 2.258 | 2.181 | 0.5337 | 0.5342 |
| 0.30 | 70.38 | 2.296 | 2.207 | 0.5342 | 0.5337 |
| 0.20 | 100 | 2.000 | 2.000 | 0.5410 | 0.5410 |
| 0.20 | 97.12 | 2.029 | 2.023 | 0.5401 | 0.5405 |
| 0.20 | 89.8 | 2.127 | 2.102 | 0.5389 | 0.5389 |
| 0.20 | 75.71 | 2.243 | 2.194 | 0.5364 | 0.5369 |
| 0.20 | 68.30 | 2.317 | 2.254 | 0.5356 | 0.5357 |
| 0.10 | 100 | 2.000 | 2.000 | 0.5440 | 0.5440 |
| 0.10 | 97.97 | 2.020 | 2.018 | 0.5429 | 0.5436 |
| 0.10 | 74.50 | 2.255 | 2.230 | 0.5385 | 0.5392 |

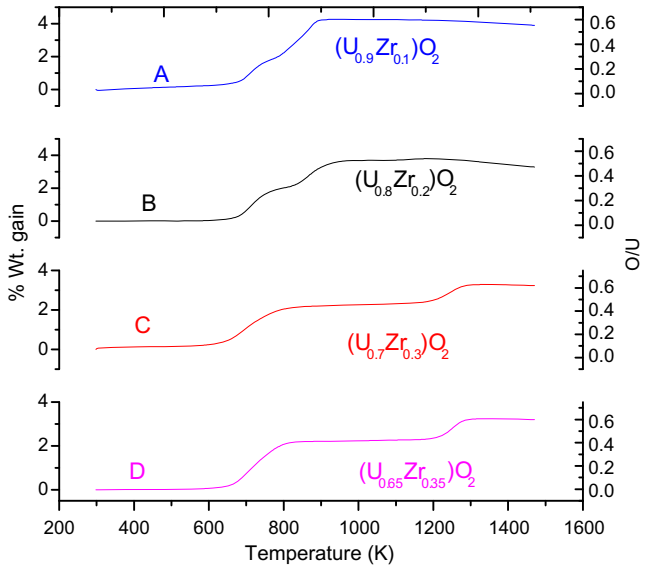


**Fig. 3.** Weight percentage gain (or O/U) against temperature plot of $Zr_yU_{1-y}O_2$ ($y$ = 0.1, 0.2, 0.3 and 0.35) in air.

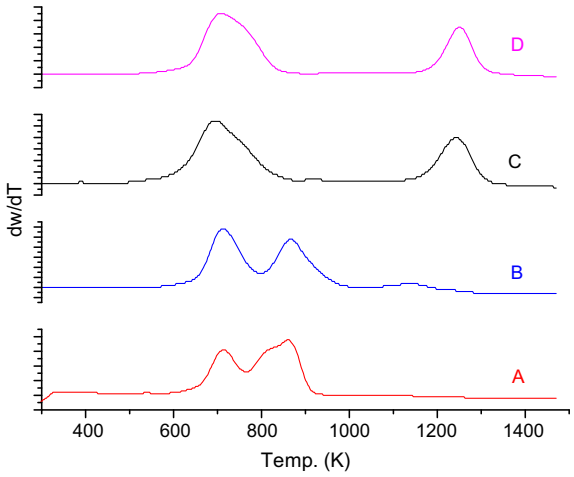


**Fig. 4.** DTG of $Zr_yU_{1-y}O_2$ for (A) $y$ = 0.1 (B) $y$ = 0.2, (C) $y$ = 0.3 and (D) $y$ = 0.35 in air.

**Table 2**
Thermogravimetric studies on $Zr_yU_{1-y}O_2$ ($y$ = 0.1, 0.2, 0.3, 0.35 and 0.4) in air.

| S. No. | Starting material | Heat treatment temperature (K) | End product | Wt gain (%) | Lattice parameter (nm) |
|---|---|---|---|---|---|
| I | $(Zr_{0.1}U_{0.9})O_2$ | 773 | $(Zr_{0.1}U_{0.9})O_{2+x}$ | 1.70 | 0.5405(2) |
| | | 1473 | $(\alpha\text{-}U_3O_8)_{ss}$[a] | 4.12 | $a$ = 0.6766(1) |
| | | | | | $b$ = 1.1899(2) |
| | | | | | $c$ = 0.4120(3) |
| II | $(Zr_{0.2}U_{0.8})O_2$ | 673 | $(Zr_{0.2}U_{0.8})O_{2+x}$ | 0.68 | 0.5389(1) |
| | | 1073 | $(\alpha\text{-}U_3O_8)_{ss}$[a] | 3.86 | $a$ = 0.6746(1) |
| | | | | | $b$ = 1.1825(2) |
| | | | | | $c$ = 0.4111(1) |
| | | 1473 | $ZrO_2 + (\alpha\text{-}U_3O_8)_{ss}$[a] | 3.53 | $a$ = 0.6759(1) |
| | | | | | $b$ = 1.1856(6) |
| | | | | | $c$ = 0.4120(1) |
| III | $(Zr_{0.3}U_{0.7})O_2$ | 750 | $(Zr_{0.3}U_{0.7})O_{2+x}$ | 1.00 | 0.5351(3) |
| | | 873 | $ZrU_2O_7 + U_3O_8$ | 2.34 | – |
| | | 1473 | $ZrO_2 + (\alpha\text{-}U_3O_8)_{ss}$[a] | 3.18 | – |
| IV | $(Zr_{0.35}U_{0.65})O_2$ | 673 | $(Zr_{0.35}U_{0.65})O_{2+x}$ | 0.97 | 0.5333(4) |
| | | 873 | $ZrU_2O_7$ | 2.21 | $a$ = 0.5168(2) |
| | | | | | $b$ = 0.5485(2) |
| | | | | | $c$ = 0.5556(2) |
| | $ZrU_2O_7$ | 1473 | $ZrO_2 + (\alpha\text{-}U_3O_8)_{ss}$[a] | 0.88 | – |
| V | $(Zr_{0.4}U_{0.6})O_2$[b] | 700 | $(Zr_{0.4}U_{0.6})O_{2+x}$[b] | 0.52 | 0.5327(2) |
| | $(Zr_{0.4}U_{0.6})O_2$[b] | 873 | $ZrU_2O_7 + ZrO_2$ | 1.45 | – |

[a] Solid solution of $ZrO_2$ in $\alpha$-$U_3O_8$ phase.
[b] Contamination of the phase with $ZrO_2$.

0.5405(2) nm and 0.5389(1) nm having O/U close to 2.25 for $y$ = 0.1 and 0.2, respectively. These data show that the fluorite type solid solutions are stable in air up to 773 K forming $Zr_yU_{1-y}O_{2+x}$ and stability of fluorite phase increases with increase in Zr concentration. These results are in agreement with reported results that $UO_2$ doped with Na, Li, Gd or Pu stabilizes fluorite phase up to 800 K [5,23,24]. The XRD pattern of the 1000 K heated product was similar to that of $\alpha$-$U_3O_8$ except for some shift in $2\theta$ to higher value indicating incorporation of $ZrO_2$ into the $U_3O_8$ structure. The solubility of $ZrO_2$ in $\alpha$-$U_3O_8$ has been reported by Pepin and McCarthy [25]. However, the solubility limit has not been given. Our study shows solubility of 20 mol% of $ZrO_2$ in $U_3O_8$ structure at 1000 K. When $Zr_yU_{1-y}O_2$ ($y$ = 0.1 and 0.2) was further heated above 1000 K, the weight loss was due to the formation of $U_3O_{8-x}$. The XRD pattern of 1473 K heated product matches with a mixture of tetragonal phase of $ZrO_2$ and zirconium substituted $U_3O_8$ indicating decrease in solubility of $ZrO_2$ at higher temperature. The data obtained for lattice parameter and volume of the unit cell showed that solubility is reduced to about 11 mol% at 1473 K. Similar observations were reported for cerium solubility in $U_3O_8$ during oxidation of mixed urania-ceria solid solutions [26]. Table 2 gives the products identified at different temperatures on heating $Zr_yU_{1-y}O_2$ ($y$ = 0.1–0.4) in air up to 1473 K together with % weight gain and lattice parameters of the single phase end product.

Figs. 3(C) and (D) and 4(C) and (D) show respectively, TG and DTG plots for oxidation of $Zr_yU_{1-y}O_2$ in air for $y$ = 0.30 and 0.35. The analysis of TG and DTG curves indicates oxidation in two steps in the temperature ranges 473–873 K and 1173–1373 K. XRD patterns of 1473 K heated products of both $y$ = 0.30 and 0.35 revealed a mixture of $ZrO_2$ and solid solution of $ZrO_2$ with $\alpha$-$U_3O_8$. The oxidized products at 873 K were found to be $ZrU_2O_7$ (O/U ≈ 2.5) for $y$ = 0.35 and a mixture of $ZrU_2O_7$ and $U_3O_8$ for $y$ = 0.3. The synthe-

sis, characterization and crystal structure of $ZrU_2O_7$ has been recently reported by us [27]. DTG curves 4C and 4D in the temperature range 473–873 K were found to be broad, so XRD patterns of 750 and 673 K heated products of $y = 0.3$ and 0.35 were recorded and found to be of fluorite type with lattice parameters 0.5351(3) nm and 0.5333(4) nm, respectively. These results show that oxidation of $Zr_yU_{1-y}O_2$ ($y = 0.3$ and 0.35) in air leads to the formation of $ZrU_2O_7$ via fluorite phase $Zr_yU_{1-y}O_{2+x}$ and the value of $x$ depends on time and temperature of heating which alters the oxygen content thereby changing the lattice parameter. It has been reported from XRD data that oxidation of pure $UO_2$ powder proceeds via $U_3O_7$ (tetragonal phase), whereas when $UO_2$ was doped with 25 mol% $PuO_2$, face-centered cubic phase, $M_4O_9$ (M = U + Pu) was formed, even when the material was heated up to 1073 K [24].

The effect of addition of $ZrO_2$ to $UO_2$, which is inert to oxidation, on the incorporation of interstitial oxygen into the lattice of $UO_2$ was also investigated. Oxidation kinetics of $Zr_yU_{1-y}O_2$ for $y = 0.2$ and 0.35 was studied in air by thermogravimetry under non-isothermal heating conditions using heating rate of 4 K/min up to 950 K. Oxidation of $UO_2$ sintered in Ar/8%$H_2$ atmosphere up to 1673 K for 10 h was also studied for comparison. Fig. 5 displays fraction oxidized ($\alpha$) with temperature for oxidation of $Zr_yU_{1-y}O_2$ ($y = 0$, 0.2 and 0.35) in air. The fraction oxidized ($\alpha$) is given by

$$\alpha = (W_t - W_0)/(W_f - W_0), \quad (5)$$

where $W_t$, $W_0$ and $W_f$ are masses at time $t$, initial mass and mass after completion of reaction, respectively. The XRD patterns of oxidized products of $Zr_yU_{1-y}O_2$ for $y = 0$, 0.2 and 0.35, at 950 K, correspond to $U_3O_8$, Zr substituted $\alpha$-$U_3O_8$ and $ZrU_2O_7$, respectively. Fig. 5 shows that oxidation of $Zr_yU_{1-y}O_2$ proceed slowly at the initial stage of reaction and the rate of oxidation increases sharply after certain temperature, with a final tailing off at the end of the experiment. This display of sigmoidal reaction kinetics is characteristic of the nucleation-and-growth mechanism of the $U_3O_8$ formation. It is also seen that as Zr concentration increases, the oxidation temperature decreases indicating decrease in thermal stability of zirconium substituted $UO_2$ in air. This can be explained as when $(U,Zr)O_2$ solid solutions were oxidized in air initially zirconium gets oxidized to $ZrO_2$ and get separated from $(U,Zr)O_2$. This $ZrO_2$ layer is porous and allows faster penetration of oxygen through $ZrO_2$ layer. Thus as zirconium concentration in $(U,Zr)O_2$ solid solutions increases more and more porous $ZrO_2$ layers were formed leading to faster oxidation of remaining oxide and this assumption is supported from the more negative oxygen potential values with increase in zirconium concentration in $(U,Zr)O_2$ solid solutions. The thermal stability of $M_yU_{1-y}O_{2+x}$ (M = Th and Gd) solid solutions has been reported to increase with increase in dopants concentration [9]. Choi et al. [28] have reported that incorporation of Th or Gd in $UO_2$ increases (more positive value) the oxygen chemical potential, $\Delta\mu$ ($O_2$), however, addition of Zr decreases oxygen potential of $UO_2$. This shows that as zirconium concentration in $Zr_yU_{1-y}O_2$ solid solutions increases, its oxidizing tendency increases as compared to that of $UO_2$ thereby decreasing the thermal stability in air.

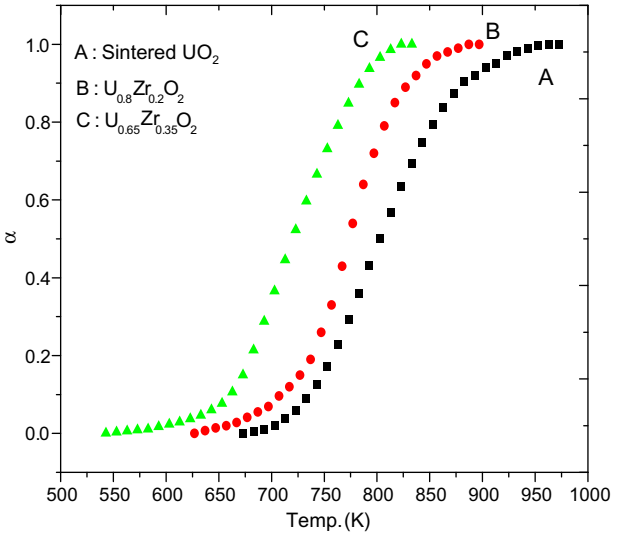


**Fig. 5.** $\alpha$ vs. temperature plots for oxidation of $Zr_yU_{1-y}O_2$ ($y = 0$, 0.2 and 0.35) in air.

The procedure for obtaining the kinetic parameters and mechanism by non-isothermal heating condition, using thermogravimetric data, has been reported earlier [5]. In this, the method suggested by Zsako [29] and computer program developed by Ravindran [30] was used for analysis. The mechanism, activation energies and pre-exponential factors obtained for the oxidation of $Zr_yU_{1-y}O_2$ ($y = 0$, 0.2 and 0.35) in air are given in Table 3. The sigmoidal nature of $\alpha$ against temperature plots (Fig. 5) and data given in Table 3 show that oxidation of the solid solutions follows nucleation and growth mechanism, Mampel type (random nucleation), as followed from the relation $g(\alpha) = -\ln(1-\alpha)$ for $y = 0$ and 0.35 with activation energy values 99 and 94 kJ/mol, respectively. The nucleation and growth mechanism observed for oxidation of $Zr_{0.2}U_{0.8}O_2$ to Zr substituted $\alpha$-$U_3O_8$ follows Avrami–Erofeev equation with $g(\alpha) = [-\ln(1-\alpha)]^{1/3}$ having activation energy value of 79 kJ/mol.

The oxidation kinetics of sintered $UO_2$ to $U_3O_8$ is reported to be temperature dependent and controlled by nucleation and growth mechanism with activation energies of 143 and 109 kJ/mol in the temperature ranges 523–623 K and 623–673 K, respectively [31]. The oxidation of $UO_2$ doped with zirconium proceeds via the sequence:

$$MO_2 \rightarrow M_4O_{9+x} \rightarrow M_3O_8 \quad (M = U + Zr). \quad (6)$$

In the nucleation and growth model, when $MO_2$ (M = U + Zr) is heated in air, the surface of the sample is oxidized to fluorite $M_4O_9$ phase almost immediately and then nucleation of $M_3O_8$ occurs on the $M_4O_9$ layer. It has been suggested that formation of cracks associated with volume change during first step of Eq. (6) leads to the formation of $M_3O_8$ nuclei. The rate of nucleation is assumed to be proportional to surface area of un-reacted material. After $M_3O_8$ nucleus has formed, its rate of growth is assumed to be isotropic and subsequent growth of $M_3O_8$ nuclei continues until the fraction converted to $M_3O_8$ approaches unity.

### 3.3. Heat capacity measurements

Specific heat capacities of $Zr_yU_{1-y}O_2$ where $y = 0.1$, 0.2, 0.3 and 0.35 were measured from 334 to 860 K using differential scanning calorimeter. Arita et al. [16] has already measured the heat capacity values of $(U_{0.91}Zr_{0.09})O_2$ by direct heating pulse calorimetry in the temperature range 290–1410 K. The specific heat capacity values for different compositions of $UO_2$–$ZrO_2$ solid solutions were plotted as a function of temperature along with $UO_2$ (s) [18] and

**Table 3**
Kinetics of oxidation of sintered $Zr_yU_{1-y}O_2$ in air for $y = 0$, 0.2 and 0.35

| Starting compound | End product | $\alpha$-range | Mechanism | $E_a$ (kJ/mol) | $Z$ ($s^{-1}$) |
|---|---|---|---|---|---|
| $UO_2$ | $\alpha$-$U_3O_8$ | 0.1–0.9 | MAMP[a] | 99 ± 10 | $5.7 \times 10^3$ |
| $(Zr_{0.2}U_{0.8})O_2$ | Zr doped $\alpha$-$U_3O_8$ | 0.1–0.9 | AE3[b] | 79 ± 8 | $4.7 \times 10^2$ |
| $(Zr_{0.35}U_{0.65})O_2$ | $ZrU_2O_7$ | 0.1–0.9 | MAMP[a] | 94 ± 10 | $1.6 \times 10^4$ |

[a] MAMP (Mampel): $g(\alpha) = -\ln(1-\alpha)$.
[b] AE3 (Avrami–Erofeev): $g(\alpha) = [-\ln(1-\alpha)]^{1/3}$.

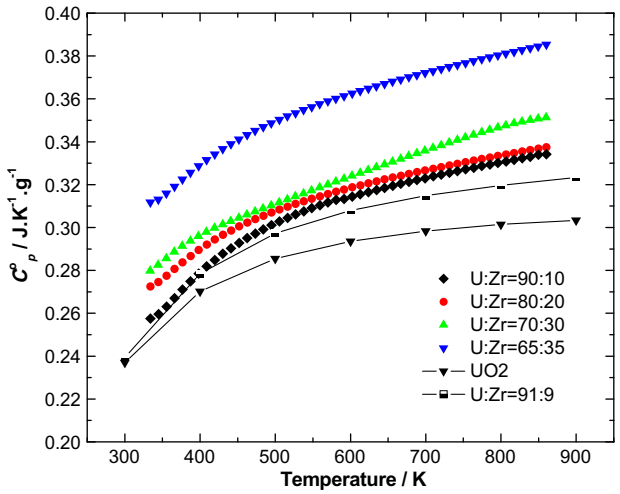


**Fig. 6.** Heat capacity of $Zr_yU_{1-y}O_{2.00}$ ($y$ = 0.1–0.35) from this study, un-doped $UO_2$ [18] and $Zr_{0.09}U_{0.91}O_{2.00}$ [16].

**Table 4**
Specific heat capacities of $Zr_yU_{1-y}O_{2.00}$ ($y$ = 0.1, 0.2, 0.3 and 0.35) as a function of temperature (K)

| $C_p$ (J K$^{-1}$ g$^{-1}$) | $Zr_yU_{1-y}O_{2.00}$ | | | | |
|---|---|---|---|---|---|
| | $y$ = 0.09 [16] | $y$ = 0.1 | $y$ = 0.2 | $y$ = 0.30 | $y$ = 0.35 |
| A | 0.3213 | 0.3212 | 0.3125 | 0.2771 | 0.3475 |
| B | +0.00001 | +0.00003 | +0.00004 | +0.00009 | +0.00005 |
| C | −7776.4 | −8440.8 | −6033.8 | −3007.3 | −6280.7 |

$C_p = A + BT + C/T^2$.

for $(U_{0.91}Zr_{0.09})O_2$ from the literature [16] and are shown in Fig. 6. The figure depicts that the temperature dependence of the heat capacities of $UO_2$ doped with $ZrO_2$ are similar to that of un-doped $UO_2$. It was found that with decreasing concentration of $ZrO_2$(s) in $UO_2$–$ZrO_2$ solid solution, heat capacity values tend to approach towards $UO_2$ values and heat capacity value of $(U_{0.90}Zr_{0.10})O_2$ from our study agrees well with that of $(U_{0.91}Zr_{0.09})O_2$. There is in no anomalous increase in the heat capacity curve of $Zr_yU_{1-y}O_2$ ($y$ = 0.1–0.35) in contrast to those of $UO_2$ doped with La, Gd and Sc [32]. The individual values of heat capacities of different compositions were fitted by the least squares method as a function of temperature in the form of polynomial expression $A + BT + C/T^2$ and values of the coefficients A, B and C are given in Table 4.

## 4. Conclusions

The conclusions from the present work on uranium–zirconium oxide solid solutions, $Zr_yU_{1-y}O_2$, can be summarized as follows:

1. The maximum solubility of 35 mol% of $ZrO_2$ in $UO_2$ lattice is obtained at 1673 K by heating $UO_2$ and $ZrO_2$ mixture initially in mild oxidizing atmosphere followed by heating in reducing environment.
2. The lattice parameter of fluorite type solid solutions, $Zr_yU_{1-y}O_2$, can be expressed as: $a_0$ (nm) = 0.54704 – 0.021$x$ – 0.030$y$.
3. The maximum solubility of zirconium oxide in $\alpha$-$U_3O_8$ phase was found to be 20 mol% at 1073 K and about 11 mol% at 1473 K.
4. The thermal stability of $Zr_yU_{1-y}O_2$ in air decreases with increase in Zr concentration. This decrease of stability is attributed to
   (i) formation of porous $ZrO_2$ layer which allows faster diffusion of oxygen leading to rapid oxidation of remaining oxide and
   (ii) decrease of oxygen potential due to addition of Zr in $UO_2$.
5. Thermogravimetric curves of oxidation of $Zr_yU_{1-y}O_2$ in air displayed sigmoidal reaction kinetics which follows the nucleation and growth mechanism for the formation of $U_3O_8$ up to 1073 K.
6. The heat capacity of $Zr_yU_{1-y}O_2$ solid solutions decreases with decrease in Zr concentration and heat capacity of $(Zr_{0.1}U_{0.9})O_2$ is close to that of un-doped $UO_2$.

## Acknowledgements

The authors are thankful to Dr V. Venugopal Director, Radiochemistry and Isotope Group and Dr S. Kannan, Head, X-ray and Structural Studies Section of Fuel Chemistry Division for their keen interest in this work.

## References

[1] I. Cohen, R.M. Berman, J. Nucl. Mater. 18 (1966) 77.
[2] N.R. Mulford, F.H. Ellinger, J. Am. Chem. Soc. 80 (1958) 2023.
[3] T. Yamashita, N. Nitani, K. Ohuchi, T. Muromura, T. Tsuji, H. Inagaki, T. Kato, J. Alloys Compd. 213/214 (1994) 375.
[4] T. Yamashita, Report JAERI 1310 (1988).
[5] S.K. Sali, S. Sampath, V. Venugopal, J. Nucl. Mater. 232 (1996) 23.
[6] J.O.A. Paschoal, H. Kleykamp, F. Thummler, J. Nucl. Mater. 151 (1987) 10.
[7] M. Yashima, T. Koura, Y. Du, M. Yashimura, J. Am. Ceram. Soc. 79 (1996) 521.
[8] W.L. Gong, E. Lutze, R.C. Ewing, J. Nucl. Mater. 277 (2000) 239.
[9] T. Fujino, C. Miyake, in: A.J. Freeman, C. Keller (Eds.), Handbook of Physics and Chemistry of Actinides, Elsevier, Amsterdam, 1991, p. 155.
[10] K. Une, M. Oguma, J. Am. Ceram. Soc. 66 (1983) C-179.
[11] I. Cohen, B.E. Schaner, J. Nucl. Mater. 9 (1963) 18.
[12] S. Aronson, J.C. Clayton, J. Chem. Phys. 35 (1961) 1055.
[13] Y. Hinatsu, T. Fujino, J. Solid State Chem. 60 (1985) 244.
[14] S. Aronson, J.C. Clayton, J. Chem. Phys. 32 (1960) 749.
[15] M. Hoch, F.J. Furmen, in: Thermodynamics, Proc. Symp. 1965, vol. 2, IAEA, Vienna, 1966, p. 517.
[16] Y. Arita, T. Matsui, S. Hamada, Thermochim. Acta 253 (1995) 1.
[17] W. Davies, W. Gray, Talanta 11 (1964) 1203.
[18] M.W. Chase, Jr. JANAF Thermochemical Tables, 4th Ed., J. Phys. Chem. Ref. Data, Monograph No. 9, 1995.
[19] Y. Hinatsu, T. Fujino, J. Solid State Chem. 60 (1985) 195.
[20] T. Yamashita, T. Fujino, J. Nucl. Mater. 132 (1985) 192.
[21] H. Nickel, Nukleonik 8 (1966) 366.
[22] R.J. McEachern, P. Taylor, J. Nucl. Mater. 254 (1998) 87.
[23] L.E. Thomas, R.E. Einziger, H.C. Buchanan, J. Nucl. Mater. 201 (1993) 310.
[24] V.J. Tennery, T.G. Godfrey, J. Am. Ceram. Soc. 56 (1973) 129.
[25] J.G. Pepin, G.J. McCarthy, J. Am. Ceram. Soc. 64 (1981) 511.
[26] H.P. Nawada, P. Sriramamurti, K.V. Govind Kutty, S. Rajgopalan, R.B. Yadav, P.R. Vasudeva Rao, C.K. Mathews, J. Nucl. Mater. 139 (1986) 19.
[27] S.K. Sali, N.K. Kulkarni, K. Krishnan, S.N. Achary, A.K. Tyagi, J. Solid State Chem. 181 (2008) 1859.
[28] J.W. Choi, R.J. McEachern, P. Taylor, D.D. Wood, J. Nucl. Mater. 230 (1996) 250.
[29] J. Zsako, J. Phys. Chem. 72 (1968) 2406.
[30] P.V. Ravindran, Thermochim. Acta 39 (1980) 135.
[31] D.G. Bose, T.T. Vandergraaf, Nucl. Technol. 32 (1977) 60.
[32] T. Matsui, Y. Arita, K. Naito, Solid State Ionics 49 (1991) 195.